



Deep learning method for 3-DOF motion prediction of unmanned surface vehicles based on real sea maneuverability test

Jiankun Lou ^a, Hongdong Wang ^{a,*}, Jianyao Wang ^a, Qing Cai ^b, Hong Yi ^a

^a MOE Key Laboratory of Marine Intelligent Equipment and System, Shanghai Jiao Tong University, Shanghai, 200240, PR China

^b Jiangsu Automation Research Institute, Lianyungang, 222061, China



ARTICLE INFO

Keywords:

Ship motion in real sea
Deep learning
Feature engineering
Maneuverability test

ABSTRACT

Motion prediction in a real sea area is a relatively difficult problem due to the lack of reliable measurement of the environment and an accurate model of ship motion under external disturbance. A deep learning method is applied in this study for the modeling of 3-DOF motion prediction under a real sea environment with the influence of currents and waves. The network with angle feature and the network with trigonometric feature are validated for the identification of the influence of the environment regarding winds, waves, and currents, in which the selection of activation function is further discussed. The developed method is validated by learning the data generated through the turning test of JARI-USV in a real sea area in Rizhao, Shandong. Analysis on the turning radius and the drift distance of the integrated track shows maximum relative errors of 5.44% and 9.09%, and the derived drift angle has a maximum absolute error of 4.84°. The prediction results verify the ability of the designed network to capture the environment influence on ship motion, as well as the turning feature of the ship itself from the maneuvering test data in a real sea trial.

1. Introduction

With the development of intelligent systems for unmanned surface vehicles (USVs), ship dynamics has become increasingly important in the iteration and renewing processes of algorithms in the systems, such as planning and control algorithms (Zhou et al., 2020). The maneuvering performance of ships in calm water has attracted great concern and thus achieved a relatively accurate stage, while that in a real sea environment with complicated wind, wave, and current is still a difficult problem. Simplified models with part of disturbance included have also been developed to deal with the problems in specific scenes. However, for the cases in which the USVs should work in a real sea environment, the lack of appropriate model of external disturbance makes it difficult to perform the algorithm tuning process.

Traditional models, such as the maneuvering modeling group (MMG) model and the Abkowitz model, have been developed and widely applied in discussing the maneuvering motion of ships. The Abkowitz model originated from the development of the Taylor series expansion, in which the nonlinear terms of elements for describing forces and moments can be expressed in a polynomial form (Abkowitz, 1980). In the MMG model, the external hydrodynamic forces and moments

exerted into the hull are decomposed, which makes it clearer to show the influence of rudder and propulsion (Kose and Saeki, 1979). The above explicit forms of ship dynamic models have led to a consequent discussion: the identification of model parameters.

Part of model parameters can be derived using an empirical formula or a previous database, which is highly limited by prior knowledge (Stern et al., 2011). Thus, dynamic model tests, such as a towing test in calm water, are among the most applied methods to verify the parameters of a ship dynamic model. Computational fluid dynamic simulations have played an important role in the process. For instance, the Reynolds-averaged Navier–Stokes solver “SURF” was applied to generate motion data for the identification of a complete set of parameters in the MMG model (Sakamoto et al., 2019). In discussing the above process, many statistical approaches, such as the improved least square method and the Kalman filter algorithm, were applied to achieve an accurate estimation of parameters (Qin and Zhang, 2014). Moreover, machine learning techniques were implemented in the process. For example, support vector machine (SVM) was widely used in parameter identification (Luo and Zou, 2009), and its improved methods, such as least square SVM, were applied in parameter estimation (Jian et al., 2015). Nevertheless, the scale effect remains one of the vital issues that

* Corresponding author.

E-mail address: whd302@sjtu.edu.cn (H. Wang).

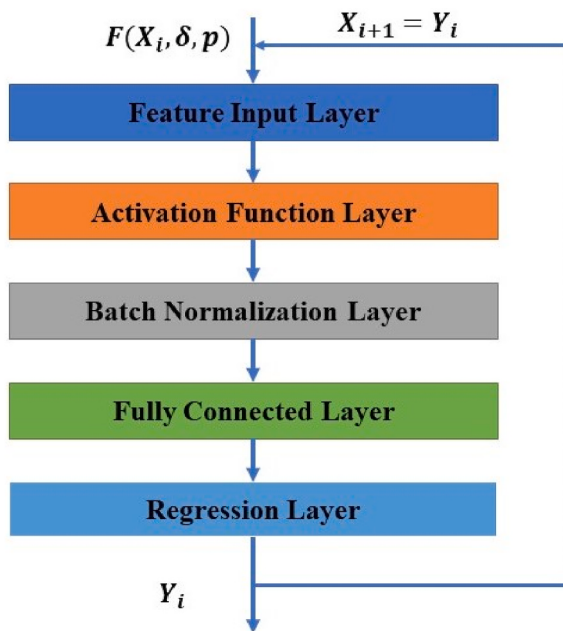


Fig. 1. Architecture of a deep learning network.

should be overcome, especially for USVs. Model tests greatly differ from the actual performance of a ship in a real sea area; thus, the derived parameters are always useless when the model is applied to describe the motion of a real-scale ship.

Accurate model descriptions of external disturbance are, however, a vital part in the above methods that cannot be well solved, which may lead to a prior error in the model. The performance of calm-water ship dynamics is highly limited in a noisy environment. Previous studies on seakeeping and maneuvering analyses have evaluated the model separately via parametric models or numerical tests. Nonetheless, analysis of the interactions between wind, wave, and current and the ship body is still difficult to conduct. A two-time scale model was unified for the analysis of ship motions in regular waves, especially linear waves and mean second-order waves (Skejic and Faltinsen, 2008; Yasukawa et al., 2021). In addition, a “hybrid approach,” in which the equation of motion was expressed by hydrodynamic coefficients, including seakeeping- and maneuvering-related coefficients, was suggested (Fossen, 2011b); the analysis of wave influence was verified in the frequency domain.

The common feature of the methods mentioned above is that they all greatly depend on a given model, which is so-called white-box model. Given that the explicit model of ship dynamics is limited by the identification of parameters, nonparametric methods, such as a black-box model, were applied in the modeling of ship dynamics. For example, Gaussian process regression was applied in system identification, and the approach turned to be accurate and robust with input noise (Xue et al., 2020). Kernel-based support vector regression is also a capable selection for the nonparametric modeling of ship dynamics (Wang et al., 2020). The mentioned methods are generally statistical methods with shallow layers, which are limited to verify a complicated nonlinear projection. However, regarding the ship maneuvering in a real sea area, the complicated environment makes the ship dynamics difficult to identify.

Deep learning methods, as a result of the development in computer performance, are advanced methods for the modeling of a physical process with high nonlinearity and strong disturbance. For instance, a long short-term memory neural net was applied to learn the interactions between nonlinear wave propagations and nonlinear roll of a ship (Xu et al., 2021). Further studies on how to apply the analysis of physical features to the design of a deep learning network were also performed. Specifically, Lyapunov stability was added in the regulation of a deep

learning network, which highly improved the generalization capability and reduced the uncertainty in the prediction of fluid flow (Erichson et al., 2019). In consideration of the limited work on the nonparametric modeling of ship dynamics by using deep learning networks on the basis of real sea trails, this paper introduces a deep learning network architecture with input feature design that relates the discussion on ship dynamics and external disturbance. The architecture turns to be an effective approach for the prediction of ship motions, including environment influence.

The rest of this paper is organized as follows. In Section 2, a deep learning network architecture is introduced, and the discussions on the activation function and input feature design are presented. In Section 3, the turning test in a real sea area based on JARI-USV, together with data measurement, is discussed, and the simulation results based on the prediction of networks with different activation functions and input features are elucidated. In Section 4, conclusions on the capability of deep learning networks for the prediction of ship motions are indicated, and further perspectives on developing network performance are provided.

2. Deep learning network design

2.1. Network architecture

The use of a deep learning network is an effective way to verify the implicit relationship in a complicated process. With the development of calculation capability, the performance of a network with a deeper architecture is more effective. In this study, the proposed architecture of a deep learning network is composed of feature input, activation, batch normalization, fully connected, and regression layers, as shown in Fig. 1.

The feature input layer is the data collector for the neural network, and global data normalization is performed. The activation function layer applies the selected activation function to the layer input to obtain a high-dimensional representation. In fact, the activation function works as a mathematical operation in the hidden layers, and the explicit form here is to emphasize the importance of selection of activation function. The appropriate selection of activation function is a fundamental step in building the network because it greatly influences the gradient features during the training process. In consideration of the boundedness and continuity of the USV dynamic model, two activation functions are selected and compared in this study. One is the clippedReLu function, which is written as

$$f_1(x) = \begin{cases} \text{ceiling } x > \text{ceiling} \\ x & 0 < x < \text{ceiling} \\ 0 & x < 0 \end{cases} \quad (1)$$

where the value of ceiling can be changed. The other is the tanh function, which is written as

$$f_2(x) = \frac{e^x - e^{-x}}{e^x + e^{-x}} \quad (2)$$

It can be derived from the translation of a sigmoid function.

The batch normalization layer is added in the architecture for the better convergence in the training progress (Ioffe and Szegedy, 2015). The calculation in this layer can be validated as follows:

$$\left\{ \begin{array}{l} \mu_B = \frac{1}{m} \sum_{i=1}^m x_i \\ \sigma_B^2 = \frac{1}{m} \sum_{i=1}^m (x_i - \mu_B)^2 \end{array} \right. \quad (3)$$

where μ_B and σ_B is the mean and variance of input data in a mini batch generated from training set $\{(x_i, y_i)\}$, and m is the size of each mini batch. Then, the output of minibatch is calculated by

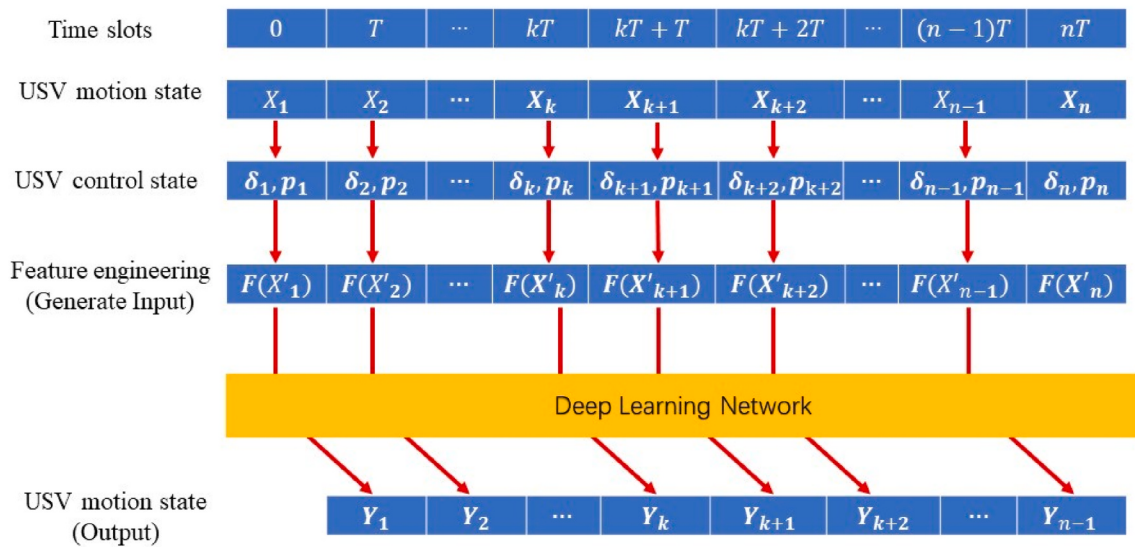


Fig. 2. Transition stage of the network for training.

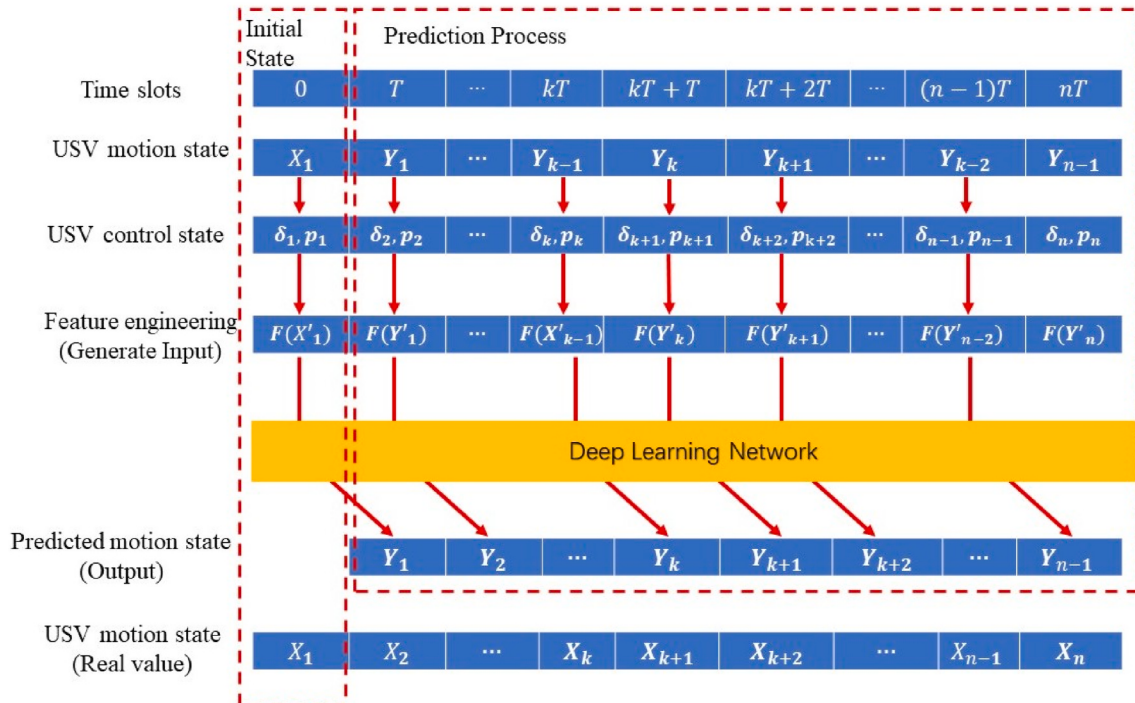


Fig. 3. Transition stage of the network for prediction.

$$y_{B,i} = \gamma \hat{x}_i + \beta, \hat{x}_i = \frac{x_i - \mu_B}{\sqrt{\sigma_B^2 + \epsilon}} \quad (4)$$

In which $y_{B,i}$ is the output of batch normalization layer and (γ, β) are learnable parameters in the layer such that will be optimized during the training process.

The fully connected layer is composed of two sublayers with extended width W to improve the capability of the proposed network. Simulation results show that different activation functions with diverse widths of layers can achieve similar prediction results, which will be shown in Subsection 3.2. Lastly, the regression layer uses the mean-squared-error loss for the evaluation task, which is written as

$$\text{MSE} = \sum_{i=1}^N \frac{\|t_i - y_i\|_2^2}{N} \quad (5)$$

where m is the number of observations, t_i is the real value of output in the observation, and y_i is the predicted output of the network. Then, a first-order gradient-based optimization of stochastic objective functions, Adam, is applied to optimize the weights and bias values in the network, where the values are initialized randomly at the beginning of training (Kingma and Ba, 2014). Meanwhile, an L2 regulation element is added to the loss function to reduce the effect of overfitting (Robert, 2014).

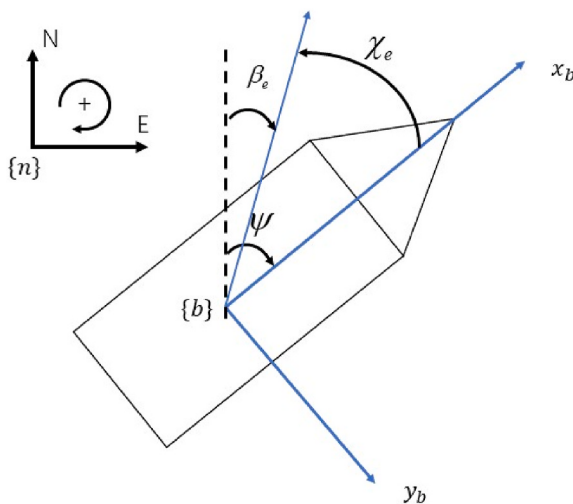


Fig. 4. Environmental force direction and corresponding relative angle.

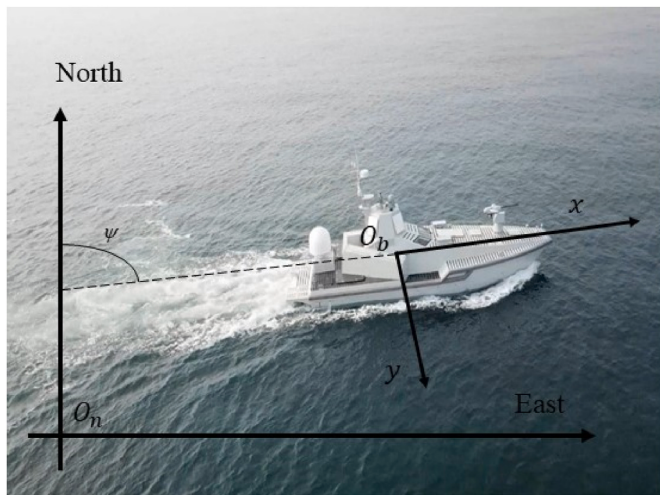


Fig. 5. JARI-USV.

Table 1
Principal dimension of JARI-USV.

Length overall (L_{OA})	15.0 m
Draft (T)	0.8 m
Light-ship displacement (W_{Light})	20 t
Maximum speed (V_{max})	42 kN
Maximum endurance (W_{en})	500 miles (in the speed of 30 kN)
Full-load displacement (W_{full})	23.5 t

Table 2
Environment information.

Sea state	Wave height	Wind level	Wind speed	Wind direction
Level 2	0.5 m	Level 3	4.5 m/s	Southeast

Table 3
Indices and settings of turning tests.

Test indices	(a)	(b)	(c)	(d)	(e)	(f)
Rudder angle $\delta (\alpha)$	15	15	20	20	25	25
Engine speed p (rpm)	650	700	650	700	650	700

2.2. Training process versus prediction process

The proposed deep learning network is designed to verify the transition process in cascaded time slots with the same sample interval, as shown in Fig. 2.

T is the sample interval of the motion state of the ship, and $\mathbf{X}_i = \mathbf{Y}_{i-1} (2 \leq i \leq n)$ denotes the motion state of JARI-USV. Regarding the 3-degree motion of USV, a simple view of \mathbf{X} can be expressed as

$$\mathbf{X} = [u, v, r] \quad (6)$$

where u , v , and r denote the surge, sway, and yaw velocities in the body-fixed reference frame, respectively. Considering the previous parametric models that calculate the motion state of ship time slot by time slot, one pair of 3-DOF motion state and the corresponding control state should be enough to calculate the current force and moment matrices to get the motion in the next time slot. However, the motion state $(\mathbf{x}_i, \mathbf{y}_i)$ is unnecessarily the exact input of the deep learning network to make the prediction of motion state in next time slots. In machine learning, feature selection is a widely used feature engineering process; this study extends \mathbf{X} into a higher dimension (Tang et al., 2014). In this way, the network may perform a better approximation process of motion prediction. The feature selection in this problem will be discussed in Sub-section 3.3. The corresponding rudder angle and main engine speed are also added as part of input features, which represent the external force generated by control signal.

During the training process, the consequent motion states are generally regarded as the input of the feature engineering process and the output of the deep learning network, that is

$$(\mathbf{x}_i, \mathbf{y}_i) = (\mathbf{F}(\mathbf{X}'_i), \mathbf{Y}_i) \quad (7)$$

where $(\mathbf{x}_i, \mathbf{y}_i)$ is one training sample, \mathbf{x}_i and \mathbf{y}_i are the input and output, respectively.

The training process is terminated when the value of the preset loss function is no longer reducing. The termination condition indicates that the prediction error of an individual input can be relatively small. That is, the simultaneous prediction from current measurement is of high accuracy. However, for a long-term prediction, the output of the network is regarded as the input of the next prediction stage, as shown in Fig. 3.

Regarding to the evaluation of the performance of a network, the simultaneous precision of prediction can always be guaranteed as the training loss during the training process is minimized. However, the error in the last prediction stage can also influence the precision of prediction in the next stage. In this case, although the prediction error in a single stage, such as

$$e = \|\mathbf{X}_i - \mathbf{Y}_{i-1}\|, \quad i \geq 2 \quad (8)$$

Can be relatively acceptable, the cumulative error in predicting the motion state can be amplified as time slots are moving. Similar problem can also appear in some parametric model in ship motion prediction, for example, an inappropriate selection of time interval of integration can lead to a divergence of ship motion state. In this case, a long-term view of ship motion should be considered, where the motion track of the target USV is generated from the integration of motion state, written as

$$\begin{cases} x_n = \sum_{i=1}^n T(u_i \sin \psi_i + v_i \cos \psi_i) \\ y_n = \sum_{i=1}^n T(u_i \cos \psi_i - v_i \sin \psi_i) \end{cases} \quad (9)$$

In which the cumulative error may also be integrated, and the motion track can be divergence.

Hence, the proposed deep learning network should be validated in not only simultaneous prediction but also long-term prediction.

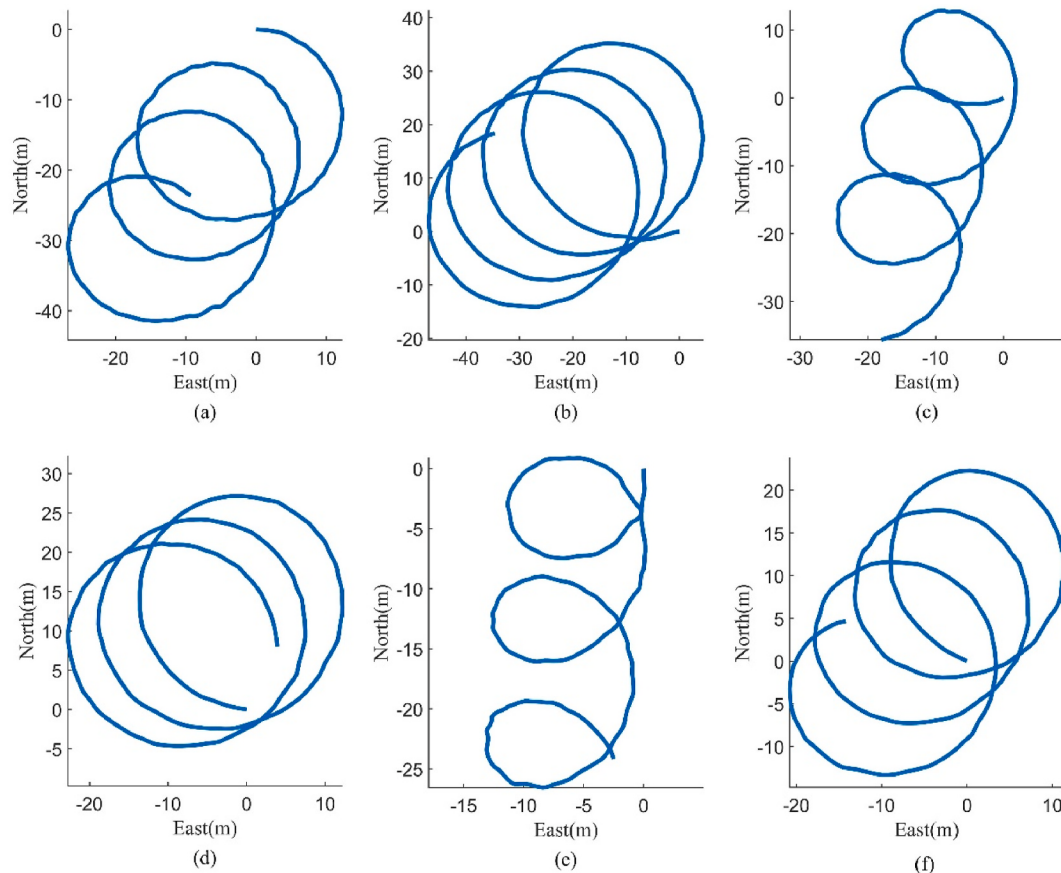


Fig. 6. Recorded track of the turning test: (a) $\delta = 15, p = 650$, (b) $\delta = 15, p = 700$, (c) $\delta = 20, p = 650$, (d) $\delta = 20, p = 700$, (e) $\delta = 25, p = 650$, (f) $\delta = 25, p = 700$.

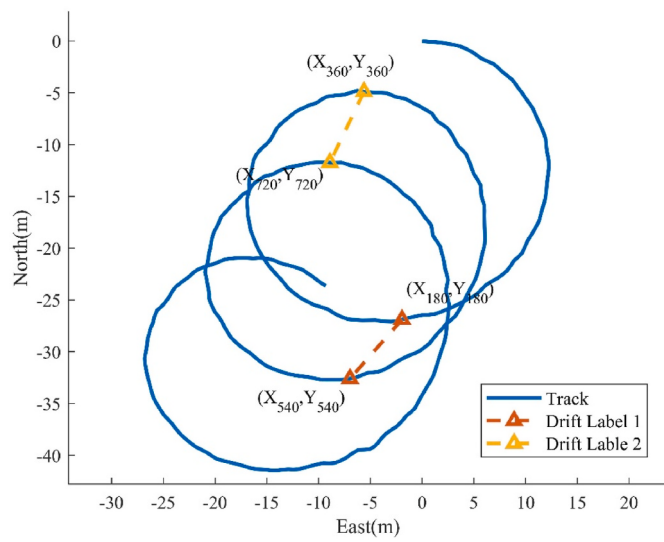


Fig. 7. Definition of drift distance.

Table 4
Drift angle in degree of measured data.

Test indices	(a)	(b)	(c)	(d)	(e)	(f)
Drift angle α_{drift} (\circ)	213.54	235.63	204.45	239.43	186.97	223.06
Drift distance d_{drift} (m)	7.60	8.36	12.60	5.21	9.78	6.63

Table 5
Options for the training process.

Options	Value
Initial Learning Rate	0.005
Mini Batch Size	128
L2 Regularization	0.0001
Maximum Epoch	500
Number of Hidden Layers	2
Number of Hidden Unit in each Layers	100

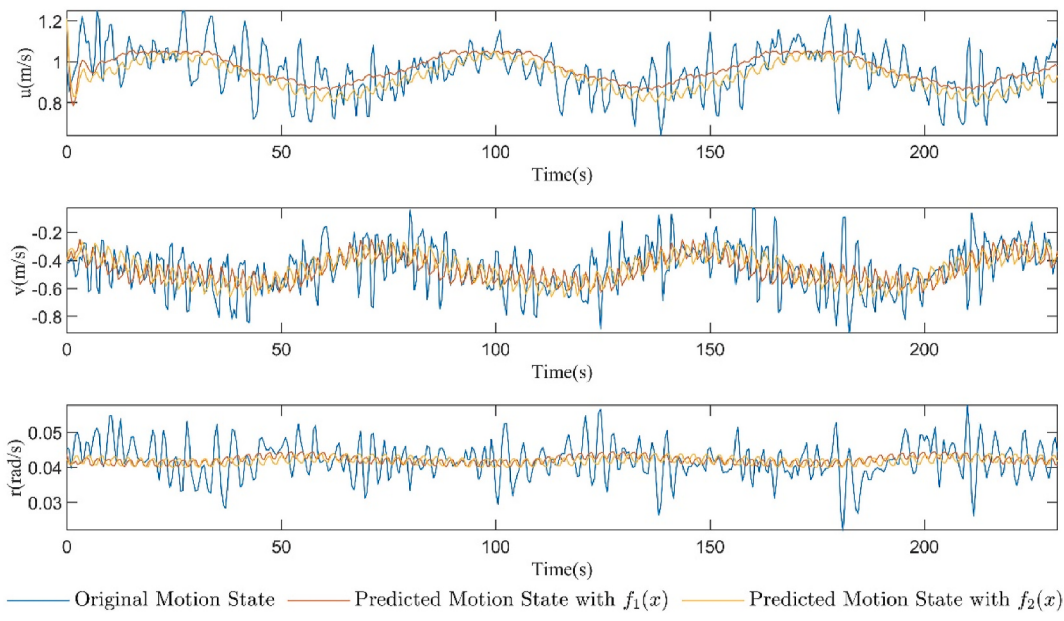


Fig. 8. Real and predicted motion data of turning test: $\delta = 15$, $p = 650$ with activation functions $f_1(x)$ and $f_2(x)$.

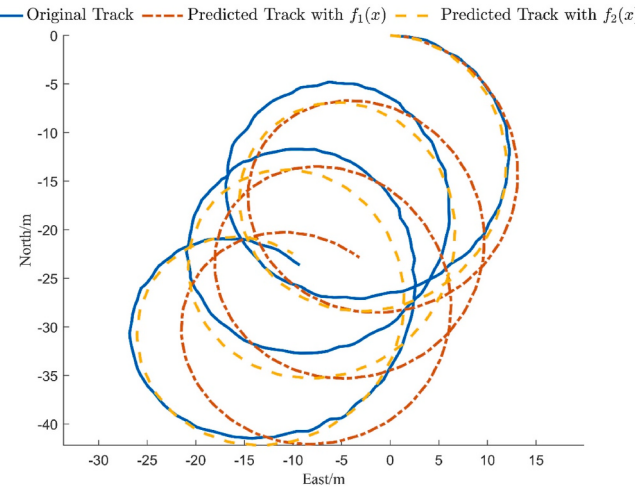


Fig. 9. Motion track for real and predicted data of turning test: $\delta = 15$, $p = 650$ with activation functions $f_1(x)$ and $f_2(x)$.

2.3. Input feature design

Feature engineering is the process of transforming raw data into features that better represent the underlying problem to predictive models, resulting in improved model accuracy in prediction. Previous studies on the MMG model or Abkowitz model have concluded that the simultaneous motion state of USV can greatly influence the parameters of the parametric dynamic model. For example, usual Abkowitz expression hydrodynamic forces of 3 DOF in calm water are shown as

Table 6
Comparison on drift angle and drift distance with different activation functions.

Dataset	Original data	Predicted data from the network of $f_1(x)$	Predicted data from the network of $f_2(x)$
Drift angle (α)	213.54	204.98	214.33
Drift distance (m)	7.60	7.42	8.29

In which the coefficients for USV in a real sea area are difficult to verify (Yao et al., 2021). On the basis of the above formula, the prediction of motion state is undoubtedly dependent on the current motion state $\mathbf{X} = [u, v, r]$ and control state $[\delta, p]$, which can be observed from the record of the inertial measurement unit (IMU) sensor directly, written as

$$F_0(\mathbf{X}) = [u, v, r, \delta, p] \quad (11)$$

Compared with the maneuvering test in calm water, real sea trials lead to a significant environment influence on the final track of the turning test. Previous studies have presented detailed discussions on the motion of ships with the influence of wind, current, and wave, which are summarized as follows:

(1) Wind-induced force and moment

For a ship with a forward moving speed, the 3-DOF force and moment expression is

$$\tau_{wind} = \frac{1}{2} \rho_a V_{rw}^2 \begin{bmatrix} C_X(\gamma_{rw}) A_{Fw} \\ C_Y(\gamma_{rw}) A_{Lw} \\ C_N(\gamma_{rw}) A_{Lw} L_{OA} \end{bmatrix} \quad (12)$$

$$\begin{aligned} X_{calm} &= X_0 + X_u \Delta u + X_{uu} (\Delta u)^2 + X_{uuu} (\Delta u)^3 + X_{\dot{u}} \dot{u} + X_v v + X_{vv} v^2 + X_{vsv} v^3 + X_r r + X_{rr} r^2 + X_{rrr} r^3 + X_{\delta\delta} \delta^2 + X_{\delta\delta\delta} \delta^3 + X_{vr} vr + X_{v\delta} v\delta + X_{r\delta} r\delta + N_{rr\delta} r^2 \delta \\ Y_{calm} &= Y_0 + Y_u v + Y_{vv} v^2 + Y_{vsv} v^3 + Y_v \dot{v} + Y_r r + Y_{rr} r^2 + Y_{rrr} r^3 + Y_r \dot{r} + Y_{vrv} vr^2 + Y_{vvr} v^2 r + Y_\delta \delta + Y_{\delta\delta} \delta^2 + Y_{\delta\delta\delta} \delta^3 + Y_{u\delta} \Delta u \delta + Y_{v\delta} v \delta^2 + Y_{r\delta} r \delta^2 + Y_{rr\delta} r^2 \delta + N_{rr\delta} r^2 \delta \\ N_{calm} &= N_0 + N_u v + N_{vv} v^2 + N_{vsv} v^3 + N_v \dot{v} + N_r r + N_{rr} r^2 + N_{rrr} r^3 + Y_r \dot{r} + N_{vrv} vr^2 + N_{vvr} v^2 r + N_\delta \delta + N_{\delta\delta} \delta^2 + N_{\delta\delta\delta} \delta^3 + N_{u\delta} \Delta u \delta + N_{v\delta} v \delta^2 + Y_{v\delta} v^2 \delta + N_{r\delta} r \delta^2 + N_{rr\delta} r^2 \delta \end{aligned} \quad (10)$$

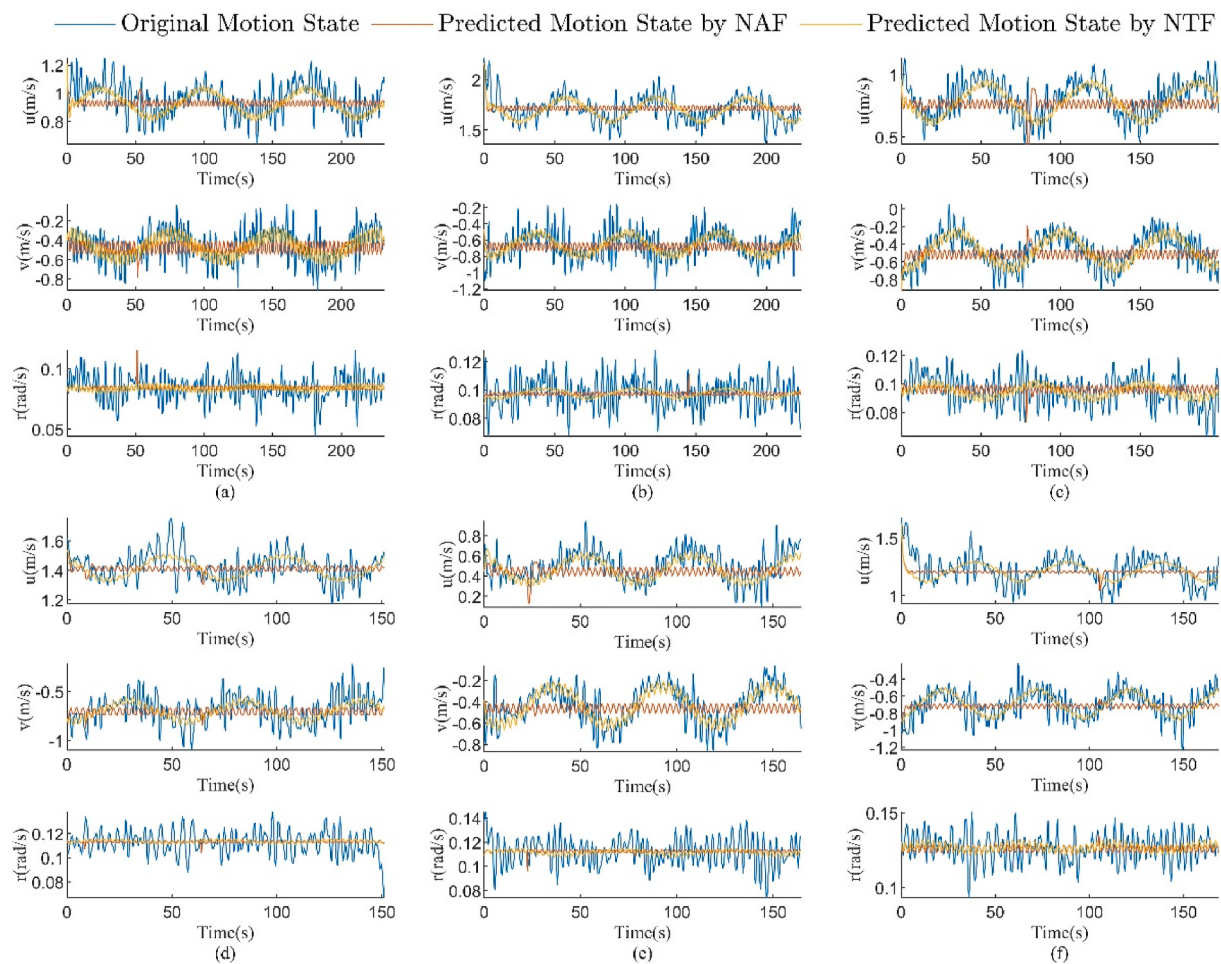


Fig. 10. Motion state comparison of measured data, predicted data by NAF, and predicted data by NTF: (a) $\delta = 15, p = 650$, (b) $\delta = 15, p = 700$, (c) $\delta = 20, p = 650$, (d) $\delta = 20, p = 700$, (e) $\delta = 25, p = 650$, (f) $\delta = 25, p = 700$.

where ρ_a denotes the air density; L_{OA} denotes the ship length overall; A_{FW} and A_{LW} denote the frontal and lateral projected areas, respectively; and C_X , C_Y , and C_N are the wind coefficients related to the wind encounter angle. The relative velocities and attack angle of wind are written as

$$V_{rw} = \sqrt{u_{rw}^2 + v_{rw}^2} \quad (13)$$

$$\gamma_{rw} = -\arctan 2(v_{rw}, u_{rw}) \quad (14)$$

The relative velocities in the body-fixed reference are written as

$$u_{rw} = u - u_{wind} \quad (15)$$

$$v_{rw} = v - v_{wind} \quad (16)$$

And the decomposition of wind velocity in the body-fixed reference is written as

$$u_{wind} = V_{wind} \cos(\beta_{wind} - \psi) \quad (17)$$

$$v_{wind} = V_{wind} \sin(\beta_{wind} - \psi) \quad (18)$$

In sum, aside from the principal dimension of the ship body, the wind forces and moments greatly depend on the wind speed and the attack angle between the direction of wind and the heading of USV.

(2) Wave-induced force and moment

The influence of waves is decomposed into different frequency

intervals. The low-frequency part induces the final motion track in the turning test in real sea, and the high-frequency part accounts for the oscillations of the measured motion states. The former part generates the common features in the integrated motion track, while the latter part shows their influence on the motion state prediction.

Regarding low-frequency waves, previous studies have evaluated wave-induced forces and moments by using Fourier coefficients written in dimensionless form as

$$F = \frac{a_0}{2} + \sum_{n=1}^i \{a_n \cos[n(\beta_{wave} - \psi)] + b_n \sin[n(\beta_{wave} - \psi)]\} \quad (19)$$

where a_n ($0 \leq n \leq i$) denotes the Fourier coefficients that are highly dependent on the wave length, and $\beta_{wave} - \psi$ is defined as the angle difference between the incident waves and ship headings (Uharek and Hochbaum, 2015; Yao et al., 2021).

(3) Current-induced force and moment

In previous parametric models, a common solution to the forces and moments from irrotational and constant currents is applying the relative velocity written as

$$\mathbf{v}_r^b = \mathbf{v}^b - \mathbf{v}_c^b \quad (20)$$

where \mathbf{v}_r^b , \mathbf{v}^b , and \mathbf{v}_c^b denote the relative velocity, USV velocity, and current velocity in body-fixed reference frame $\{b\}$, respectively (Fosset, 2011a). The body-fixed reference frame $\{b\}$ and the north-east-down

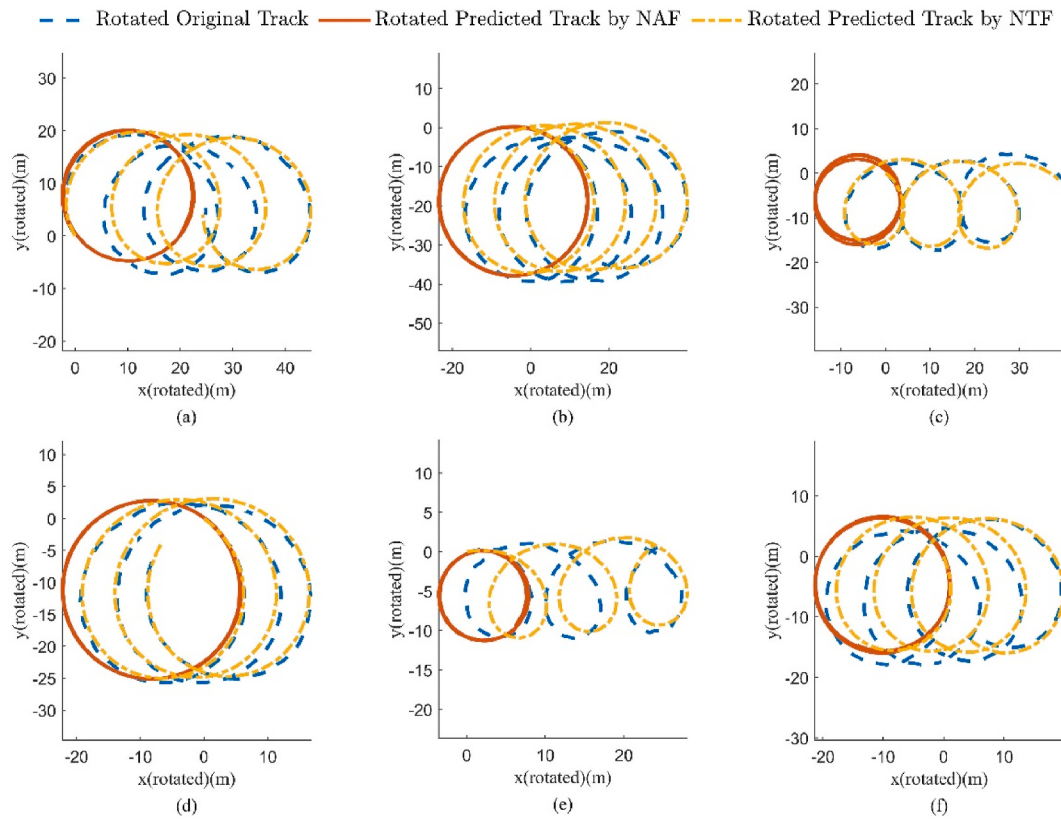


Fig. 11. Rotated track comparison of measured data, predicted data by NAF, and predicted data by NTF: (a) $\delta = 15, p = 650$, (b) $\delta = 15, p = 700$, (c) $\delta = 20, p = 650$, (d) $\delta = 20, p = 700$, (e) $\delta = 25, p = 650$, (f) $\delta = 25, p = 700$.

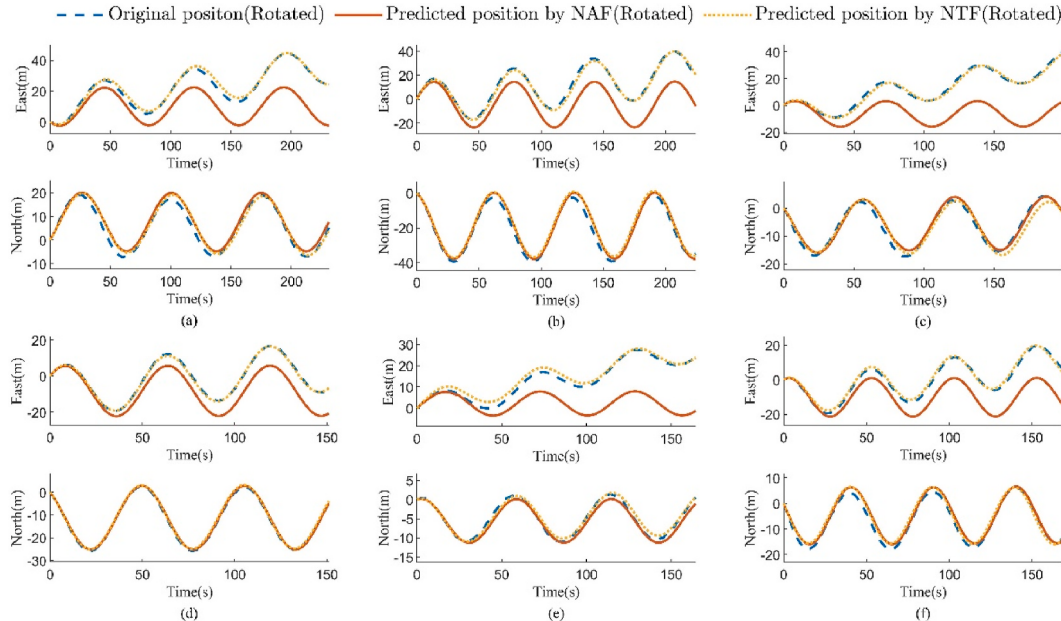


Fig. 12. Rotated position comparison of different feature generation functions: (a) $\delta = 15, p = 650$, (b) $\delta = 15, p = 700$, (c) $\delta = 20, p = 650$, (d) $\delta = 20, p = 700$, (e) $\delta = 25, p = 650$, (f) $\delta = 25, p = 700$.

coordinate system $\{n\}$ are defined and shown in Fig. 4. The current velocity defined in $\{b\}$ can be calculated through a rotation matrix, such that

$$\mathbf{v}_c^b = \mathbf{R}_n^b(\psi) \mathbf{v}_c^n$$

where $\mathbf{R}_n^b(\psi)$ denotes the rotation matrix that projects vector in $\{n\}$ to $\{b\}$, and ψ is the heading angle of USV, which is equivalent to the relative angle of $\{b\}$ relative to $\{n\}$. Suppose the direction of current is β_c , for a 3-DOF motion model, \mathbf{v}_c^b is written as

$$(21)$$

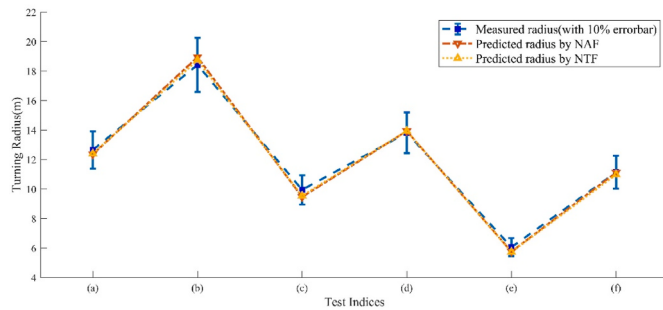


Fig. 13. Turning radius comparison in each test.

Table 7

Turning radius of turning test from measured and predicted data.

Test indices	(a)	(b)	(c)	(d)	(e)	(f)
Measured radius (m)	12.66	18.43	9.95	13.82	6.07	11.15
Predicted radius by NAF (m)	12.36	18.95	9.47	13.94	5.76	11.12
Relative error of radius by NAF	-2.38%	2.81%	-4.83%	0.87%	-5.11%	-0.25%
Predicted radius by NTF (m)	12.41	18.74	9.55	13.94	5.74	10.99
Relative error of radius by NTF	-2.01%	1.68%	-4.01%	0.91%	-5.44%	-1.43%

Table 8

Drift angle in degree of measured data and predicted data from NTF.

Test indices	(a)	(b)	(c)	(d)	(e)	(f)
Measured drift angle α_{drift} (°)	213.54	235.63	204.45	239.43	186.78	223.06
Predicted drift angle α_{drift} (°)	214.33	232.43	206.79	236.14	181.95	224.21
Absolute error of angle (°)	-0.79	3.21	-2.34	3.28	4.84	-1.15
Measured drift distance d_{drift} (m)	7.60	8.36	12.60	5.21	9.78	6.63
Predicted drift distance d_{drift} (m)	8.29	7.67	12.894	4.98	8.91	6.30
Relative error of drift distance	-9.09%	8.27%	-2.39%	4.29%	8.98%	5.08%

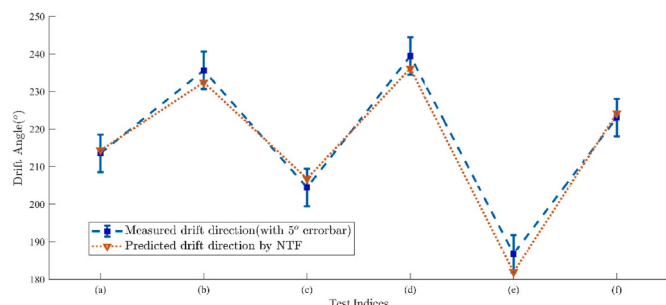


Fig. 14. Drift angle comparison in each test.

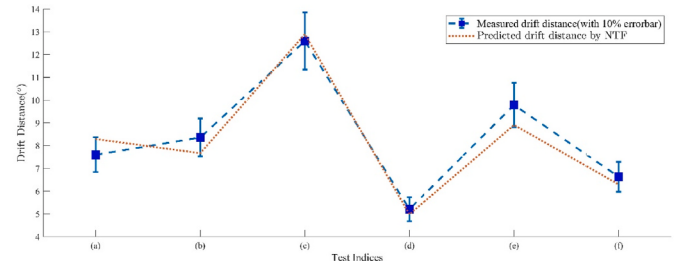


Fig. 15. Drift distance comparison in each test.

$$\mathbf{v}_c^b = \begin{bmatrix} V_c \cos(\beta_c - \psi) \\ V_c \sin(\beta_c - \psi) \\ 0 \end{bmatrix} \quad (22)$$

$V_c = \|\mathbf{v}_c^n\|$ denotes the current speed.

In summary, from previous discussions of a 3-DOF dynamic model of USV with environmental forces and moments, the related coefficients highly depend on environment measurement. However, limited methods can be used to perform an accuracy evaluation of wind velocity, current velocity, wave length, and wave direction, which makes the environment-induced influence difficult to evaluate. In this case, a deep learning method is a feasible way, considering that the parameters for describing the environment can be regarded as implicit parameters to be learned.

A consequent hypothesis can be derived on the basis of the previous discussion that the encounter angles between the heading of USV and the wind, current, and incident wave directions are vital elements in calculating the environmental forces and moments. In Fig. 4, χ_e denotes the relative angle between the environmental forces and the ship heading, which is written as

$$\chi_e \in \{\beta_{wind} - \psi, \beta_{wave} - \psi, \beta_c - \psi\} \quad (23)$$

where χ_e should be transformed in range $(-\pi, \pi]$. Hence, the heading of USV is a fundamental feature of the deep learning network to retain the effect of environment during the training process.

Thus, in accordance with the foundational form shown in Eq. (11), a possible feature generation function can be further extended into

$$\mathbf{F}_1(\mathbf{X}) = [u, v, \omega, \delta, p, \psi]^T \quad (24)$$

Such a network with angle feature (NAF) contains further information as model input, in which the previous explicit model is a factor that influences the corresponding coefficients. Moreover, the trigonometric form appears in all the expressions of environmental forces and moments, as it is a fundamental formula in the decomposition process of forces and moments. The analysis of current is regarded as an example; in consideration of Eq. (22), a sum-to-product formula can be applied, written as

$$\mathbf{v}_c^b = \begin{bmatrix} V_c (\cos \beta_c^n \cos \psi + \sin \beta_c^n \sin \psi) \\ V_c (\sin \beta_c^n \cos \psi - \cos \beta_c^n \sin \psi) \\ 0 \end{bmatrix} = \begin{bmatrix} \lambda_1 \cos \psi + \lambda_2 \sin \psi \\ \lambda_2 \cos \psi - \lambda_1 \sin \psi \\ 0 \end{bmatrix} \quad (25)$$

where $\lambda_1 = V_c \cos \beta_c^n$, and $\lambda_2 = V_c \sin \beta_c^n$. Hence, the expression of \mathbf{v}_c^b is a linear summation of $\cos \psi$ and $\sin \psi$ for V_c and β_c^n are constant values in each test. Similar analysis can be performed in relation to wind and wave. The trigonometric formula of the ship heading angle is another possible choice for the extension of input features. Then, another feature generation function is derived as

$$\mathbf{F}_2(\mathbf{X}) = [u, v, \omega, \delta, p, \sin \psi, \cos \psi]^T \quad (26)$$

In this case, a network with trigonometric feature (NTF) eliminates the possible trigonometric function projection in the model, which may reduce the complexity of the model that the network should represent.

3. Sea trials and simulations

3.1. Maneuvering turning test of JARI-USV

The USV tested is called JARI-USV, which was constructed by the Jiangsu Automation Research Institute, as shown in Fig. 5. The principal dimension of JARI-USV is listed in Table 1. The seaworthiness of JARI-USV is to work effectively in sea state 3 or less, maintain high speed in sea state 4, and maintain safe voyage in sea state 5.

Regarding the motion sensors, JARI-USV has GPS for global positioning and IMU for motion state recording. The sample frequencies of GPS and IMU are 50 and 200 Hz, respectively. IMU can record the acceleration of USV and perform the filter and integral step by itself. Previous tests have proved that the accuracy of IMU is high enough for further analysis, especially for the measurement of surge, sway, and yaw. The velocity measured by IMU in 3 DOF is defined in body-fixed reference frame $\{b\}$, and the heading ψ of USV is defined in north-east-down coordinate system $\{n\}$, which is also shown in Fig. 5.

The turning test of JARI-USV was performed in Rizhao, Shandong Province in China. The sea state was level 2, and the wave height was approximately 0.5 m. The wind velocity was approximately 4.5 m/s with the direction of southeast. During the test, the directions of wave and current kept changing with time. The above record was collected from the local meteorological website or via observation, which is summarized in Table 2.

To eliminate the influence of human control, the rudder angle and engine speed were fixed during a subtest. For the turning test, the sampled rudder angles δ were 15°, 20°, and 25°, and the sampled RPMs p were 650 and 700. The test indices are shown in Table 3.

Hence, eight tests in total were performed on that day, and each turning test lasted 3–4 min. A down sampling process from 200 Hz to 2 Hz was performed on the real measured IMU data to reduce the dataset size. The track of maneuvering tests in each case is shown in Fig. 6.

As shown in Fig. 6, the real sea environment induced a significant displacement of the turning circle, which made it difficult to verify the USV dynamics based on traditional parametric models. In a previous study that performed real environment trails, a Gaussian filter was used to move the noises in measured data to eliminate the potential disturbance (Xu et al., 2020), considering that the initial ship dynamic model is sensitive to the disturbance. However, in the current study, noises are vital parts to be learned. Meanwhile, the results of track simulation in the turning test are generally coincident with those in previous works (Uharek and Hochbaum, 2015; Yao et al., 2021).

A previous study on the influence of steady flow on a turning test evaluated the process by using drift distance (Lee and Kim, 2020). The drift distance in this paper is defined as

$$d_{drift} = \frac{1}{2} \left[\sqrt{(X_{540} - X_{180})^2 + (Y_{540} - Y_{180})^2} + \sqrt{(X_{720} - X_{360})^2 + (Y_{720} - Y_{360})^2} \right] \quad (27)$$

where (X_A, Y_A) denotes the location in the track where the heading of USV has increased by A degree compared with the initial heading, as shown in Fig. 7.

Drift angle can also be calculated by

$$\alpha_{drift} = \frac{1}{2} \left[\arctan \frac{Y_{540} - Y_{180}}{X_{540} - X_{180}} + \arctan \frac{Y_{720} - Y_{360}}{X_{720} - X_{360}} \right] \quad (28)$$

where α_{drift} denotes the drift angle, and the definition of that is the angle between the proposed direction and the north direction and in reference

$$\{n\}.$$

Then, the drift angle and corresponding drift distances in each time interval of the turning test can be verified and listed in Table 4.

3.2. Influence of activation function

As discussed in Subsection 2.1, the appropriate activation function of a deep learning network can greatly improve the network capability. For the proposed network, two typical activation functions $f_1(x)$ and $f_2(x)$ are chosen and compared. In the turning test, $\delta = 15$, $p = 650$ are selected for detailed discussion, and the feature generation function selected here is $F_2(\mathbf{X})$. Specifically, the options for the training process are summarized in Table 5.

The initial learning rate is set to 0.005 and during the training process, it will decrease accordingly. The minibatch size is set to 128 and the L2 regularization parameter is 0.0001. Based on the training loss in the process, 500 turns to be a reasonable maximum epoch. Moreover, the number of hidden layers and number of hidden units in each layer is set to 2 and 100, respectively.

On the basis of the transition stage shown in Fig. 2, the prediction result of the motion state of USV is shown in Fig. 8. The integrated track is calculated using Eq. (9) and shown in Fig. 9.

The environment influence is captured by the network, while the integrated track is exactly different with distinct activation functions. Detailed analysis can be performed in observing the predicted u varying with time. Compared with the predicted value with activation function $f_2(x) = \tanh x$, the prediction of u with activation function $f_1(x)$ seems to have an upper bound. The maximum value of u should appear where the heading of USV is along with the direction of ocean current, and the value of u keeps increasing before the stage and decreasing after the stage. Hence, the network with activation function clippedReLU cannot capture the inner projection as the USV performs the maneuvering test, whereas the network with activation function $f_2(x) = \tanh x$ leads to reasonable prediction results of motion states and integrated motion track. As depicted in Fig. 9, the global orientations of integrated track have significant differences. Detailed calculations of drift angle and drift distance can then be performed, and the results are listed Table 6.

Table 6 presents that with clippedReLU function, the integrated track has a drift distance closer to the original data, and the predicted drift angle has an unnegelectable error. On the contrary, the application of activation function $f_2(x) = \tanh x$ provides not only a closer prediction of the motion state but also a more accurate prediction of the motion track compared with the original measured data.

3.3. Ability to capture the environment influence

On the basis of the simulation results in Subsection 3.2, the activation function of the proposed network selected for feature generation analysis is $f_2(x) = \tanh x$. A similar prediction transition stage is performed for different turning tests. The same training options shown in Table 5 are applied here. The predicted 3-DOF motion state varying with time is shown in Fig. 10. The prediction of NAF in 3-DOF motion state changes slightly as the USV moves, whereas NTF makes a prediction that the motion state of USV changes periodically. Compared with the measured data, the predicted motion states turn to be smoother.

Then, the integrated motion track can be calculated using Eq. (9). The track rotated for the corresponding drift angle of measured data, the rotated tracks of original data, and the predicted tracks are shown in Fig. 11. The x axis in Fig. 11 for each turning test is parallel to the drift angle of real measured track. In this case, a clearer contrast can be specified in separately comparing how the values of x and y change with time, as shown in Fig. 12. From the two figures, the proposed network is of high convergency in long-term prediction and integrated stages. Moreover, the integrated tracks and their separate comparisons show that NTF makes a prediction closer to the real measurement, in which the environment influence of ocean current is unnegelectable. In Fig. 12,

NTF predicts a motion track closer to the original measured data in x and y axes.

3.4. Precision of final track derived

Further verification on the evaluation of the turning test can be performed. For the turning test with external ocean current, the turning radius here is defined as

$$r_t = \frac{1}{2} \overline{(y_{upper} - y_{lower})}_{circle} \quad (29)$$

where r_t is the turning radius, which is calculated by the average of the difference between the upper bound y_{upper} and lower bound y_{lower} in each circle period in the rotated track. The turning radius derived using Eq. (29) is listed in Table 6 and illustrated in Fig. 13.

The predicted turning radius is of high accuracy compared with the measured data, in which the maximum relative error is 5.44% for turning test $[\delta, p] = [25, 650]$ predicted by NTF (see Table 7). Moreover, the prediction in turning radius with various feature generation functions has no significant difference. For the prediction of NAF, although the environment influence from ocean current is eliminated, the prediction in 3-DOF velocity still shows some oscillations, as exhibited in Fig. 10. Considering that the predicted turning radius in steady state is of acceptable accuracy, NAF can be a possible selection to be applied in calm-water analysis to replace traditional regression-based models, such as the KT model. As the prediction of NTF cannot only maintain the turning properties but also shows the environment influence, NTF can replace traditional methods in correlating the environment and parametric dynamic model, in which an efficient way to verify the parameters of a model in a real sea area is lacking.

The drift angles and corresponding drift distances are evaluated using Eq. (27) and Eq. (28). The above values together with the angle from measured data in Table 4 are listed in Table 8, and the comparison plot is shown in Fig. 14 and Fig. 15. Given that NAF cannot show the influence of ocean current, Table 8 only lists the drift angle from the measured data and the predicted data from NTF. Considering the condition that the angle value is highly dependent on reference selection, this paper only discusses the absolute error of angle difference.

As shown in Table 8, the prediction of drift angle from the integration of prediction in motion states is of acceptable error, in which the maximum absolute error is 4.84° for the turning test with setting $[\delta, p] = [25, 650]$. The maximum relative error 9.09% of drift distance prediction appears in test (a). In consideration of the circumstance in a real sea environment, the external disturbance from ocean current is time varying, although the turning test lasts a limited time interval. Hence, the measured data contain complicated environment information, which makes the above error in predicting drift angle reasonable for analysis.

4. Conclusions

In this paper, a deep-learning-based method is introduced for the prediction of ship motions based on data from a real sea maneuvering turning test performed by JARI-USV. Discussion on the measured data indicates that the environment influence plays a vital role in the ship model. Previous nonparametric models focus on the transition of motion states and can be difficult to capture the disturbance feature from the environment. In this study, to address the above problems, networks with different input features, NAF and NTF, are designed for dealing with the environment information among real measured data. On the basis of the analysis of the empirical form of the forces and moments of wind, waves, and currents, the ship heading angle and its trigonometric value are added as the input feature of the network for modeling the environment influence. Furthermore, detailed discussion on the activation functions of the network is conducted to achieve better

performance in the prediction of motion state.

Numerical simulation results show that with the trigonometric function of ship heading as an additional input, NTF shows a great capability in capturing the environment influence. The predicted drift angle is close to the real measured data. Comparison on different activation functions indicates that the tanh function is a good choice for the network. In addition, turning radius, drift distance, and drift angle are selected as evaluation indicators to evaluate the performance of NAF and NTF. The simulation results present that NAF and NTF are both convergent and have the same ability in the evaluation of turning radius. However, compared with NTF, NAF cannot capture the environment influences from the test data in a real sea area and shows a prediction similar to that of a model in calm water. By contrast, NTF has great performance in predicting drift angle and drift distance, and it is a good choice to predict the ship motion state in a real sea area. Compared with previous work, the proposed methods can capture the environment influences from the motion state in a real sea trial without measuring environment labels, such as wave length and direction. It is worth mentioning that the phenomena of drifting are learned by the network itself, while in parametric model the environment influence should be specifically added. Moreover, the potential noise caused from the measurement in real condition is successfully neglected by the network during the training process, making the learning of a ship model under noisy condition easier. Thus, an alternative way is conducted for the representation of the ship model in a specific sea area. The deep learning network can learn the features of ship motion and the environment influence from the data of a real sea maneuverability test.

In summary, the proposed network shows a reliable and convergent prediction of ship motions of JARI-USV. In the future, several concerns will be further discussed. First, specified design of real sea test should be extended, such that the environment feature and ship dynamics can be better captured in measured data. Second, further research can be performed on how to model environment disturbance through adding more layers, extending the input dimension of the network, and using sequential data. Lastly, detailed prior analysis on measured data should be performed for better explanation of learning results, e.g., evaluating the measured and prediction data in the frequency domain.

CRediT authorship contribution statement

Jiankun Lou: Conceptualization, Investigation, Software, Visualization, Writing – original draft, Writing – review & editing. **Hongdong Wang:** Funding acquisition, Project administration. **Jianyao Wang:** Methodology, Validation. **Qing Cai:** Resources, Formal analysis. **Hong Yi:** Data curation.

Declaration of competing interest

The authors declare that they have no known competing financial interests or personal relationships that could have appeared to influence the work reported in this paper.

Acknowledgments

This paper is sponsored by the National Natural Science Foundation of China (51909162) and Shanghai Rising-Star Program. In addition, great appreciation is given to the Jiangsu Automation Research Institute for providing the test data of JARI-USV.

References

- Abkowitz, M.A., 1980. Measurement of hydrodynamic characteristics from ship maneuvering trials by system identification. *Trans. - Soc. Nav. Archit. Mar. Eng.* 88, 283–318.
- Erichson, N.B., Muehlebach, M., Mahoney, M.W., 2019. Physics-informed Autoencoders for Lyapunov-Stable Fluid Flow Prediction. *ArXiv abs/1905.10866*.

- Fossen, T.I., 2011a. *Handbook of Marine Craft Hydrodynamics and Motion Control*. Wiley, Chichester.
- Fossen, T.I., 2011b. A nonlinear unified state-space model for ship maneuvering and control in a seaway. *International Journal of Bifurcation and Chaos* 15 (9), 2717–2746.
- Ioffe, S., Szegedy, C., 2015. Batch normalization: accelerating deep network training by reducing internal covariate shift. In: Proceedings of the 32nd International Conference on International Conference on Machine Learning, vol. 37. JMLR.org, Lille, France, pp. 448–456.
- Jian, C., Jiayuan, Z., Feng, X., Jianchuan, Y., Zaojian, Z., Hao, Y., Tao, X., Luchun, Y., 2015. Parametric estimation of ship maneuvering motion with integral sample structure for identification. *Appl. Ocean Res.* 52, 212–221.
- Kingma, D., Ba, J., 2014. Adam: a method for stochastic optimization. *Comput. Sci.*
- Kose, K., Saeki, T., 1979. On a New Mathematical Model of Manoeuvring Motions of a Ship. *Journal of the Society of Naval Architects of Japan*, 1979.
- Lee, J.-H., Kim, Y., 2020. Study on steady flow approximation in turning simulation of ship in waves. *Ocean Eng.* 195.
- Luo, W.L., Zou, Z.J., 2009. Parametric identification of ship maneuvering models by using support vector machines. *J. Ship Res.* 53 (1), 19–30.
- Qin, Y., Zhang, L., 2014. Parametric identification of ship's maneuvering motion based on Kalman filter algorithm. *Mechatron. Automat. Cont. Syst.* 107–114.
- Robert, C., 2014. Machine learning, a probabilistic perspective. *Chance* 27 (2), 62–63.
- Sakamoto, N., Ohashi, K., Araki, M., Kume, K.-i., Kobayashi, H., 2019. Identification of KVLCC2 manoeuvring parameters for a modular-type mathematical model by RaNS method with an overset approach. *Ocean Eng.* 188.
- Skejic, R., Faltinsen, O.M., 2008. A unified seakeeping and maneuvering analysis of ships in regular waves. *J. Mar. Sci. Technol.* 13 (4), 371–394.
- Stern, F., Agdraup, K., Kim, S.Y., Hochbaum, A.C., Rhee, K.P., Quadvlieg, F., Perdon, P., Hino, T., Broglia, R., Gorski, J., 2011. Experience from SIMMAN 2008—the first workshop on verification and validation of ship maneuvering simulation methods. *J. Ship Res.* 55 (2), 135–147.
- Tang, J., Aleyani, S., Liu, H., 2014. Feature selection for classification: a review. *Data Classification: Algorithms and Applications* 37–64.
- Uharek, S., Hochbaum, A.C., 2015. Modelling Mean Forces and Moments Due to Waves Based on RANS Simulations. ISOPE, 2015.
- Wang, Z., Xu, H., Xia, L., Zou, Z., Soares, C.G., 2020. Kernel-based support vector regression for nonparametric modeling of ship maneuvering motion. *Ocean Eng.* 216.
- Xu, P.-F., Cheng, C., Cheng, H.-X., Shen, Y.-L., Ding, Y.-X., 2020. Identification-based 3 DOF model of unmanned surface vehicle using support vector machines enhanced by cuckoo search algorithm. *Ocean Eng.* 197, 106898.
- Xu, W., Maki, K.J., Silva, K.M., 2021. A data-driven model for nonlinear marine dynamics. *Ocean Eng.* 236, 109469.
- Xue, Y., Liu, Y., Ji, C., Xue, G., Huang, S., 2020. System identification of ship dynamic model based on Gaussian process regression with input noise. *Ocean Eng.* 216.
- Yao, J., Liu, Z., Song, X., Su, Y., 2021. Pure low-frequency and pure high-frequency ship motion equations in regular waves. *Ocean Eng.* 233.
- Yasukawa, H., Hasnan, M.A.A., Matsuda, A., 2021. Validation of 6-DOF motion simulations for ship turning in regular waves. *J. Mar. Sci. Technol.*
- Zhou, C., Gu, S., Wen, Y., Du, Z., Xiao, C., Huang, L., Zhu, M., 2020. The review unmanned surface vehicle path planning: based on multi-modality constraint. *Ocean Eng.* 200, 107043.